Article

Landslide Awareness System (LAwS) to Increase the Resilience and Safety of Transport Infrastructure: The Case Study of Pan-American Highway (Cuenca–Ecuador)

Pietro Miele [1], Mariano Di Napoli [2,*], Luigi Guerriero [1], Massimo Ramondini [3], Chester Sellers [4], Mariagiulia Annibali Corona [1] and Diego Di Martire [1]

1   Department of Earth, Environment and Resources Sciences, Federico II University of Naples, Complesso Universitario di Monte Sant'Angelo, 80126 Naples, Italy; pietro.miele@unina.it (P.M.); luigi.guerriero2@unina.it (L.G.); mariagiulia511@hotmail.it (M.A.C.); diego.dimartire@unina.it (D.D.M.)
2   Department of Earth, Environment and Life Sciences, University of Genoa, 16132 Genoa, Italy
3   Department of Civil, Architectural and Environmental Engineering, Federico II University of Naples, 80125 Naples, Italy; massimo.ramondini@unina.it
4   Instituto Ecuatoriano de Regimen Seccional (IERSE), University of Azuay, EC-01.01.981, Cuenca 010107, Ecuador; csellers@uazuay.edu.ec
*   Correspondence: mariano.dinapoli@edu.unige.it

Abstract: In most countries, landslides have caused severe socioeconomic impacts on people, cities, industrial establishments, and lifelines, such as highways, railways, and communication network systems. Socioeconomic losses due to slope failures are very high and they have been growing as the built environment expands into unstable hillside areas under the pressures of growing populations. Human activities as the construction of buildings, transportation routes, dams, and artificial canals have often been a major factor for the increasing damage due to slope failures. When recovery actions are not durable from an economic point of view, increasing the population's awareness is the key strategy to reduce the effects of natural and anthropogenic events. Starting from the case study of the Pan-American Highway (the Ecuadorian part), this article shows a multi-approach strategy for infrastructure monitoring. The combined use of (i) DInSAR technique for detection of slow ground deformations, (ii) field survey activities, and (iii) the QPROTO tool for analysis of slopes potentially prone to collapse allowed us to obtain a first cognitive map to better characterize 22 km of the highway between the cities of Cuenca and Azogues. This study is the primary step in the development of a landslide awareness perspective to manage risk related to landslides along infrastructure corridors, increasing user safety and providing stakeholders with a management system to plan the most urgent interventions and to ensure the correct functionality of the infrastructure.

Keywords: DInSAR; QPROTO; landslides; infrastructure monitoring; awareness system; Pan-American Highway

1. Introduction

Road networks play a key role in the economic and social development of a society, such that the maintenance of safety conditions for users is the most important challenge for the decision-makers and stakeholders. Landslide interaction with populated areas and transportation infrastructures may induce the loss of human lives and meaningful economic damage [1], both reducing road-user safety and modifying the roadway geometry [2]. In these scenarios, the detection of critical sectors along infrastructure corridors is essential [3]. These considerations are emphasized by the lack of awareness concerning natural hazards [4].

In areas where recovery actions are not sustainable from an economic point of view, the population's awareness is the key strategy to reduce the effects of natural and anthropogenic events. Landslide hazard awareness is interlinked with the community resilience

level (in terms of technical and financial capacity), especially in developing countries [5]. In order to manage risk related to landslides along infrastructure corridors, increasing user safety, it is essential to provide policymakers with awareness instruments such as landslide inventory and related susceptibility maps with potential information related to stability conditions of slopes along hillsides [6–8].

In these conditions, landslide consequences need to be examined through either (i) impact assessment analysis, focused on cost surveys or risk analyses [9,10], or (ii) vulnerability assessments, where the sensitivity to landslide damage is often studied starting from technical reports and from a retrospective point of view [11,12].

In the last decades, structural and infrastructural health monitoring with differential interferometry SAR (DInSAR) [13] technique has become one of the most powerful and economic methodologies [14–16]. In particular, DInSAR has been widely used in landslide identification and infrastructures monitoring involved with slow and very slow mass movements since it captures data covering wide areas [17–22]. Thanks to the short temporal baseline and the relatively low costs of acquisition and processing procedures, interferometric tools have grown as one of the most important and valuable methods for the investigation of unstable areas. Actually, the possibility of detecting areas affected by deformation phenomena makes it possible to estimate the instability proneness of urbanized areas or transport infrastructures in a timely manner and with sufficient precision at the same time.

Unfortunately, in many cases, infrastructures are also affected by rapid phenomena such as falls and topples [23–25]. It is known that DInSAR technique allows exploratory study on the comprehensive rock mass stability and slow ground displacements, to detect and monitor possible precursory phenomena [26]. Rockfalls are usually characterized by fast velocities reducing the suitability of spaceborne DInSAR methodologies [27]. However, several studies (e.g., [28]) have pointed out the opportunity of detecting precursory deformation preceding blocks detachment in rockfalls. In this perspective, in order to be able to investigate all types of landslides (including rockfalls) that may affect urbanized areas and linear infrastructures, accounting also for their propagation mode [29], it is necessary to also implement other methodologies that allow to estimate the effects of rapid phenomena. In this regard, the use of computer tools for rockfall simulations has become popular in determining runout distance, jump height, kinetic energy, and impact force [30], and consequently identifying potential rockfall areas [31]. In this study, the QPROTO tool was used [32–34].

A relevant example of transport infrastructure corridor exposed to landslide hazard is the Ecuadorian linear infrastructure network (Pan-American Highway) [35–37]. The Pan-American Highway is located in the Andes mountain region and the roads of these territories have proved to be more prone to landsliding [38]. Since its construction, the Pan-American Highway, in particular the sector between the cities of Cuenca and Azogues, has been involved in landslides, also induced by earthquakes, with severe effects on the economy [39] and users' safety. The blocking of the Pan-American Highway breaks off several important population centers, creating a road communication emergency which affects the economy and the mobility of the population.

On these bases and considering both the frequency of landslide events and the lack of a comprehensive product for highway safety management from a landslide perspective, this work aims at providing local authorities a cognitive tool depicting slope dynamics in terms of actively moving and potential landslides affecting user safety and the correct functionality of the Pan-American Highway. The results, consisting of an updated slow-moving landslide inventory and associated prospective rockfall susceptibility scenario, can be considered as an operational landslide awareness system that might guide mitigation measurement design and slope monitoring to improve highway user safety. The last inventory update is dated 1994 [40]. In addition, the development of such a tool, based also on smart technologies [41], might have a direct impact on the local population resilience increasing landslide risk awareness.

2. Pan-American Highway Cuenca–Azogues (Troncal de la Sierra E35)

The segment of the highway analyzed in this study connects the city of Cuenca with the city of Azogues (Figure 1). Known as the South Pan-Americana, it has a length of about 22 km and has six lanes (three per direction).

Its construction began in 1995 and ended in 1997. It is one of the fundamental arteries of the city of Cuenca; according to the Ministry of Transport and Public Works [42], it is estimated an average traffic of about 46,000 vehicles per day. Since the beginning of its construction, the E35 has been affected by a large number of different types of landslides, from falls and topples to rotational and translational sliding. Such landslides have often caused damage to the infrastructure and incidents to the users, especially in winter. In some cases, such landslides caused the interruption of the road as well, with the need to remove the material that affected the highway (Figure 2b,d), even causing the deviation of the road axis (Figure 2a).

The main issues relating to artificial slope instabilities (Figure 2c) can be attributed to the techniques used during infrastructure construction, creating sub-vertical fronts without mitigation works connected. In general, it is possible to identify the triggering causes (i.e., rainfalls or/and earthquakes) and the predisposing ones, making the territory prone to instability. Rock masses are made by heterogeneous materials having different structural settings, and consequently different responses to destabilizing factors. The knowledge of the geological properties (i.e., lithology, structure, bedding, faults, tectonics, hydrogeological regime, etc.) is of primary importance and of great help for the engineering activity. Unfortunately, all these geological considerations are not always taken into account. The main cause determining problems of instability of the rocky fronts is the presence of water. It is known that the presence of infiltration water in a rock slope always represents a negative factor for stability. In fact, infiltration through fractures represents an element of considerable risk, due to possible generation of high interstitial pressures within the slope.
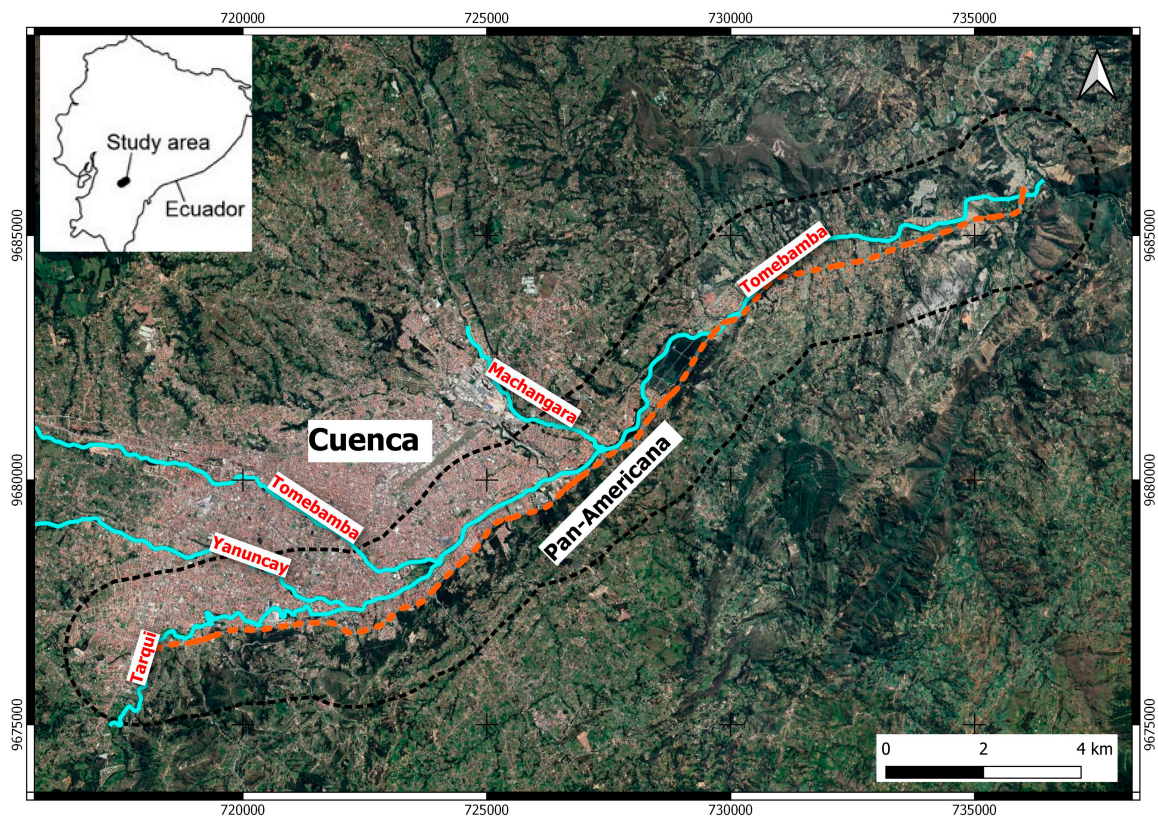

Figure 1. The Pan-American Highway between the city of Cuenca and Azogues (red dashed line) and the buffer zone surrounding the infrastructure (black polygon).

Figure 2. The functionality of the Pan-American Highway is often interrupted by rockfalls. (**a**) Deviation of the original road axis (red dotted line) caused by rockfall events; (**b**) landslide deposits have almost completely invaded the highway; (**c**) overdip cataclinal slope: the stratification is slope-oriented; (**d**) boulders detached from the slopes block the lane.

3. Geological Setting

The Cuenca area (in full, Santa Ana de los Cuatro Rios de Cuenca) is situated in the southern part of Ecuador, in the Azuay province, between the two main Andes cordilleras at an elevation ranging from 200 meters to 4500 meters above sea level. The study area is surrounded to the east by the Eastern Cordillera edge [43] and to the west by uplifted Tertiary volcanic arc piles, whose basement is very probably continental, as evidenced by crystalline outcrops west of Cuenca [44,45]. This relative depression received thick, marine to subaerial deposits [46–48]. In the first phase, the basin was filled with marine sediments and metamorphic clasts derived from the Eastern Cordillera and subsequently with coarse-grained fluvial and alluvial sediments derived from the west. In the Cuenca areas, Faucher et al. [49] and Bristow [50] identify three distinct lithologic units: cherts and greywackes; poorly consolidated shales with limestone lenses and arkosic sandstones beds, and marine shales.

The Pan-American Highway crosses, nearby the Cuenca city, the Azoguez formation (Figure 3), composed mostly of conglomerates, which provoke many instability phenomena. The dominant features of the city's geography are also the source of its name in Spanish: the four rivers of Cuenca (meaning a basin made up of a confluence of rivers). These rivers are the Tomebamba (named after the Inca culture), Yanuncay, Tarqui, and Machangara, in order of importance. The first three rivers originate in the Páramo of Parque Nacional Cajas to the west of the city. These four rivers are part of the Amazon River watershed.
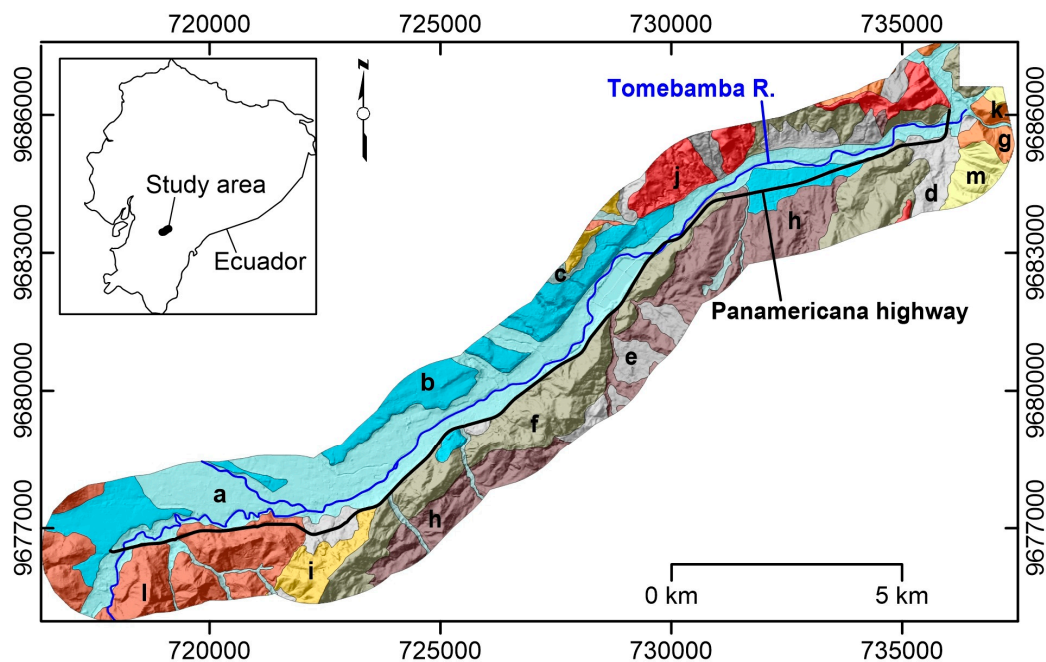
Figure 3. Geological sketch map of the Cuenca canton (Southern Ecuador): (**a**) alluvial deposits, (**b**) terrace deposits, (**c**) colluvial and alluvial deposits, (**d**) colluvial deposits, (**e**) slope deposits, (**f**) Azogues Formation, tuffaceous sandstones, (**g**) Biblian Formation, sandy clays, (**h**) Loyola Formation, laminated shales with gypsum, (**i**) Magan Formation, siltstones and conglomeratic sandstones, (**j**) Gualaceo/Llacao Formations, volcanic deposits, (**k**) Tarqui Formation, kaolinized tuffs, (**l**) Turi Formation, coarse conglomerates, (**m**) Yanguilla Formation, gray massive siltstones.

4. Materials and Methods

Operational landslide identification, from an awareness system development perspective, was executed through a multi-step procedure. As a first step, a field survey and remote-sensing analysis were realized in order to accomplish a landslide inventory as completely as possible. Subsequently, rockfall-prone areas analysis was performed thorough the cone method modeling approach.

4.1. Multi-Approach Landslide Inventory

A landslide inventory map (LIM) represents a fundamental tool to display information on landslides activity and their multitemporal evolution [9]. In most cases, inventories are discontinuous over time and so-called event-based landslide inventories are available, which are landslides inventories based on a singular severe event (rainfall, earthquake).

The LIM was derived from interferometric data and the visual interpretation of aerial photos integrated and validated by field investigation [51–55]. DInSAR allows to measure ground displacements with sub-centimetric accuracy, starting from data acquired from satellites orbiting the Earth at an average height of 600 km. The DInSAR approach is based on the analysis of phase difference in interferometric stacks of radar images. The A-DInSAR technique operates at a full spatial resolution and identifies reliable scatterers (permanent scatterers—PS) [56] by measuring their multitemporal coherence related to the phase stability. In particular, DInSAR methodology allows to analyze long data series producing mean displacement rate maps and time series of deformations along the direction between the SAR sensor and the target (line of sight—LoS). In this work, Sentinel-1A and B, ascending and descending mode images acquired in the timespan from October 2016 to May 2019 (Table 1), were processed by the SUBSIDENCE software, which uses the coherent pixel technique–temporal phase coherence (CPT–TPC) approach [57,58], and developed at the Remote Sensing Laboratory (RSLab) of the Universitat Politècnica de Catalunya of Barcelona.

Table 1. Synthetic aperture radar (SAR) imagery analyzed in the present study.

Satellite	Orbit	Time Span	Nr Scenes
Sentinel-1	Ascending	1 October 2016–25 May 2019	114
Sentinel-1	Descending	10 October 2016–16 May 2019	99

The datasets available from this study consist of 114 images acquired in ascending orbit with a time-revisiting variable between 6 and 36 days, and 99 images acquired in descending orbit with a time-revisiting variable between 12 and 96 days. Specifically, the interferometric chain implemented in SUBSIDENCE is divided into four main steps. The first is the generation and selection of interferogram and consists of selecting a quality set of interferograms, considering the temporal and spatial thresholds, from all the possible combinations among available images, in order to minimize spatial and temporal correlation which affects the results. The second step is the pixel selection, named stable coherence scatterers (SCS), characterized by a reliable phase. The temporal phase coherence (TPC) estimator was used in order to select SCS. The third one is the evaluation of the linear term of deformation to define the linear velocity and location of the targets; then the evaluation of the nonlinear deformation component and atmospheric artefacts to assess the deformation evolution of selected pixels. Finally, the geocoding of the results in WGS84 and WGS84-UTM coordinate reference systems was performed. For the last step mentioned, a high-accuracy digital elevation model (DEM) with a resolution of 3 × 3 meters was considered. The DEM was used to produce the slope map and, in a second moment, accordingly with the Pan-American Highway route, a buffer zone of 1.5 km surrounding the infrastructure was created in Geographic Information System (GIS) environment in order to isolate critical SCS around the road.

This approach allows to obtain the LoS mean displacement rate and the time series of deformations to the entire data processing interval for each SCS around the road in both acquisition geometries. After the processing step, the interferometric results were post-processed using the "Heatmap" plugin in the QGIS environment. This tool, through the application of the kernel density estimation (KDE) algorithm, allows to identify the unstable areas (UAs) affected by meaningful deformations [59–61].

Subsequently, geomorphological field surveys were carried out between November 2019 and January 2020 using 1:5000 topographical maps as a basemap, whereas visual interpretation activities were carried out on Google Earth satellite images. Data collected from the field and remote sensing activities were then georeferenced and digitized as polygons within a GIS environment. The slope failures were recognized and classified according to Cruden and Varnes [62] and Hungr et al. [63].

4.2. Identification of Potential Rockfall Sectors

Although the DInSAR technique has proven to be effective for the assessment of surface displacements with sub-centimeter accuracy and at the same time covering very large areas, it is limited to studying only phenomena that demonstrate displacement rates of less than a few tens of centimeters per year [64]. Referring to rock masses, the DInSAR technique only allows to estimate the presence of precursory phenomena of a collapse. Therefore, to better characterize the potential damage due to mass movement impact and stability analysis, QPROTO software was exploited.

QPROTO (QGIS Predictive ROckfall TOol) is a plugin developed entirely in Python language that can be run by open-source QGIS software (https://plugins.qgis.org/plugins/qproto/ accessed on 12 March 2021). The plugin aims at executing the cone method [32,65] to reproduce the rockfall phenomenon. The algorithm adopts a simplified energy assumption in which the falling block path is summarized by an equivalent sliding motion of the boulder along a straight line (i.e., the energy line) linking the more distant observed fallen block to the slope apex (i.e., the shadow angle method) [34]. The plugin applies the model by performing a viewshed analysis starting from a fixed set of viewpoints

(i.e., the rockfall source points). From each of these points of view, a visibility cone is determined in the vertical and horizontal plane through the angles φ_{P} and α that represent the energy line angle and the lateral spreading one, respectively. The first angle constitutes the main cone method parameter and has to incorporate all the information concerning the block (e.g., size and shape) and the cliff (e.g., roughness, soil type, slope, length, forest density, protection works) [34]. The angle is estimated by using the following relationship [32]:

$$\varphi_{\mathrm{P}} = \arctan\left(\left|\frac{z_{sp} - z_f}{d_{sp} - d_f}\right|\right) \tag{1}$$

where z_{sp} is the rockfall trigger point quote, z_f is the farthest location of the block elevation, and $(d_{sp} - d_f)$ is the distance between the farthest deposit point and the rockfall source.

The key parameters used to calculate the cone method phenomenon characteristics are schematically shown in Figure 4:
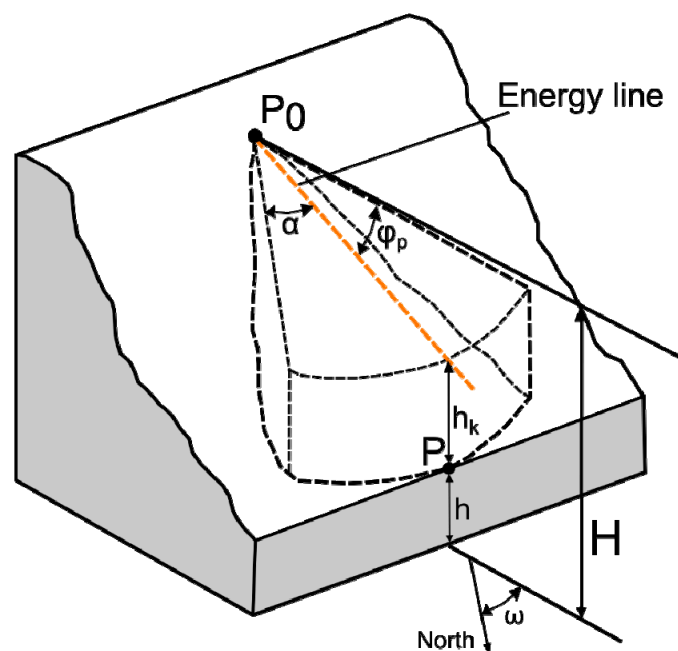

Figure 4. Schematic representation of a generic calculation section of the QPROTO algorithm.

　　　H = trigger point quote;
　　　P_0 = trigger point;
　　　P = observed block;
　　　φ_{P} = energy line angle;
　　　α = lateral spreading angle;
　　　ω = angle between the maximum slope direction and the north;
　　　h = intercept point;
　　　h_k = difference between energy line and topography;
Starting from the slope map, obtained by DEM 3×3 m data, of the region of interest, the highest acclivity areas ($>45°$) [66] were chosen to perform the QPROTO investigation. The detected areas were subsequently divided into 15 sectors to better execute the algorithm (Figure 5). The plugin provided various output maps with a preset chromatic scale that indicates the different susceptibility classes as number of occurrences. It allows to preliminarily evaluate the effects of a rockfall event along a slope in terms of exposed areas to runout boulders. The elaborations implemented with QPROTO provide different output maps directly displayed in the QGIS interface and with a preset chromatic scale which facilitates the visualization.
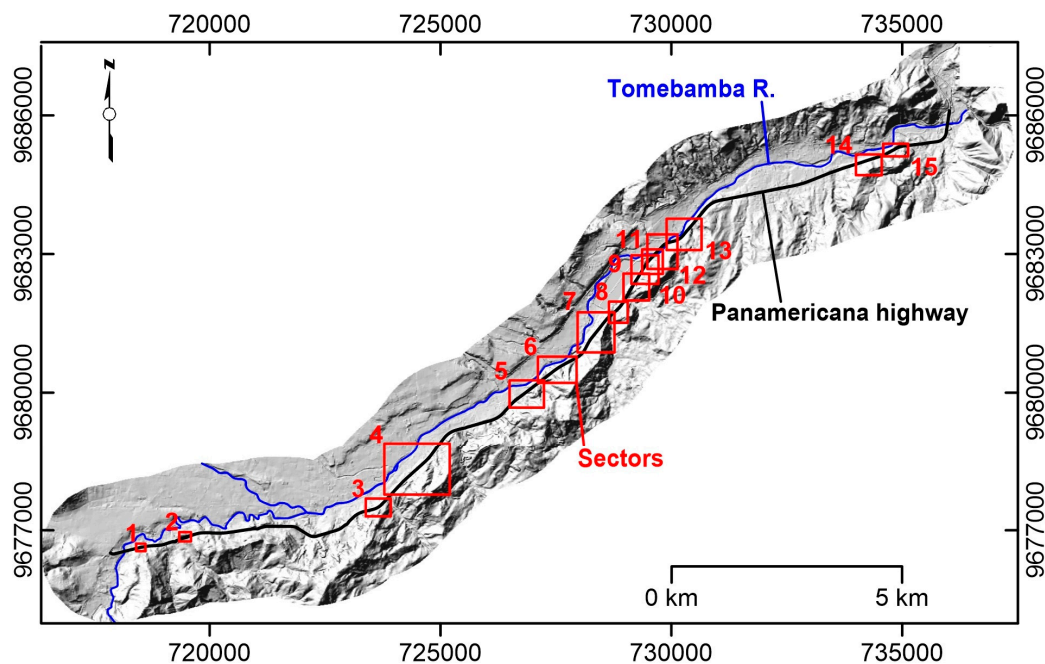
Figure 5. Red polygons correspond to sectors identified through geomorphological analysis and then used to perform QPROTO investigation. On 15 identified sectors, 12 correspond to road cuts.

5. Results

5.1. Multi-Approach Landslide Inventory

Using the CPT–TPC approach, about 78,000 SCS were detected for the ascending geometry imagery and 42,000 SCS for the descending one. Among all the obtained scatterers, only those that fall within the buffer zone surrounding the infrastructure were taken into consideration to interpret potential slope instability affecting the Pan-American Highway. In the buffer area, only the slopes that overlook the road were considered as the source of mass movements that can potentially affect it (Figure 6). Hence, two mean displacement rate maps were obtained, each for both acquisition geometries. The SCS' mean displacement rate was represented using a color scale from red to blue: the positive values, conventionally represented with blue scale color, indicate a movement of the target towards the satellite; the negative values, represented with red scale color, indicate movement far from the sensor; and the green colors indicate stable points (Figure 6). As showed in Figure 6a–c, SCS are distributed in a homogeneous way along the whole analyzed road's section. The most meaningful displacement rates, identified by blue and red points, are located in the NE sector where the pelitic and argillitic deposits outcrop (Loyola Formation).

The KDE analysis identified different clusters for both acquisition geometries. For the ascending data (Figure 6b), the kernels are mainly distributed along the central and NE sectors with high values of density. On the contrary, for the descending data (Figure 6d), the kernels detected are less frequent and show lower density values. This analysis allowed to identify only the SCS clusters that correspond to mass movements potentially involving the road's track.

Combining the KDE output and information from field surveys, a total of 141 landslides were identified and mapped within the study area surrounding the infrastructure (Figure 7). Among these, 30 landslides were recognized during the field surveys, and for the remaining deformation areas, detected through remote sensing techniques, a subsequent field validation and classification were carried out (Table 2). Detecting with this procedure, on a total length of 22 km analyzed between the cities of Cuenca and Azogues, 3.5 km have been potentially affected by slow landslides.
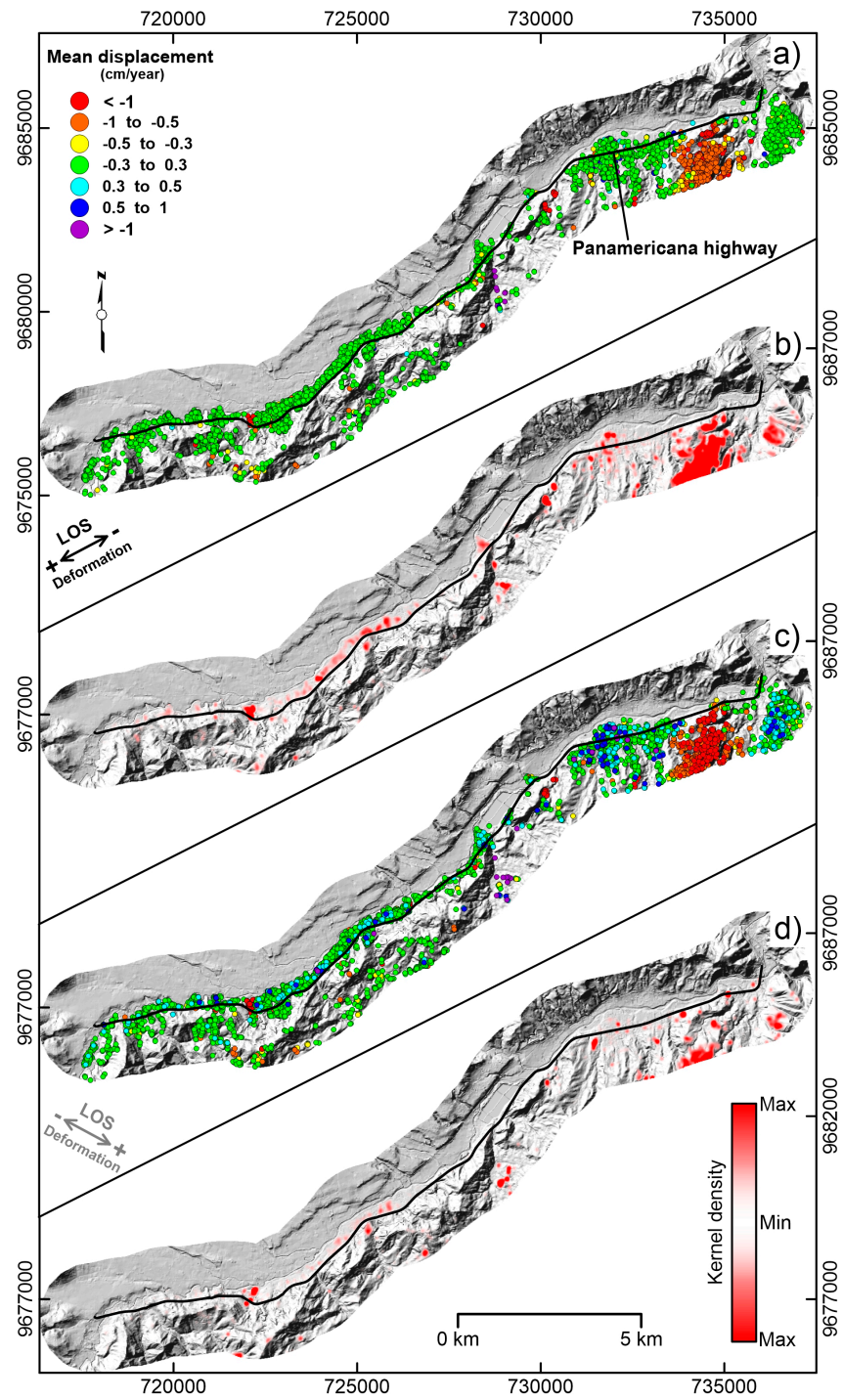
Figure 6. SCS mean displacement rate maps for ascending (**a**) and descending (**c**) acquisition geometry. The results of KDE algorithm are shown in (**b**,**d**), respectively. The biggest red cluster in the northern area visible both in ascending and descending displacements maps could be explained as a deformation movement with major component along the vertical axis.
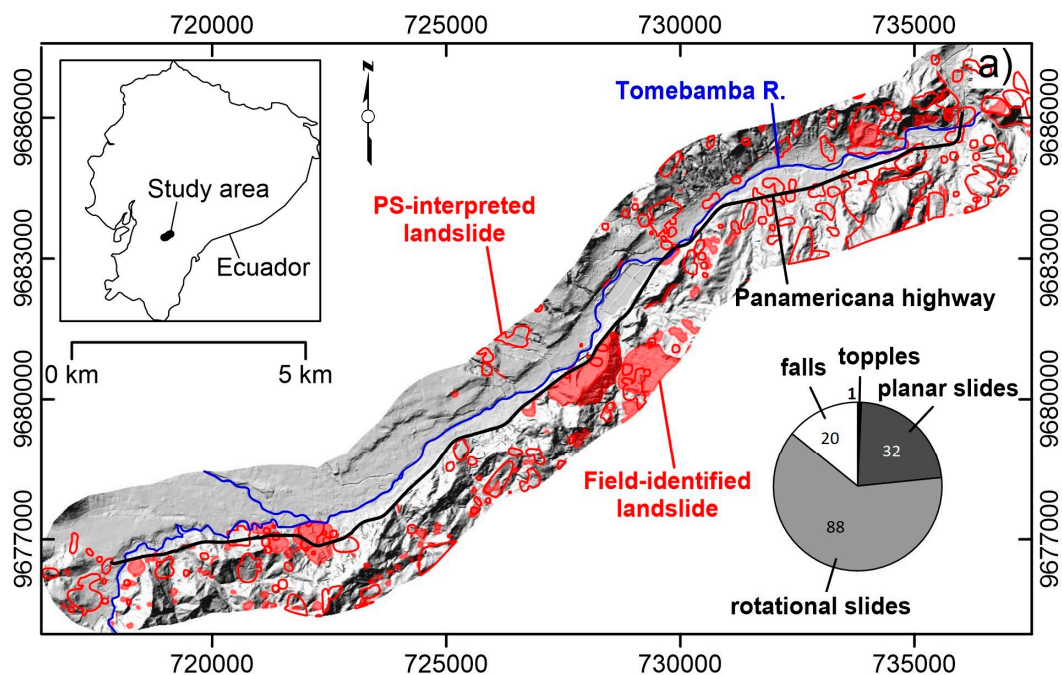
Figure 7. Mapped landslides surrounding the Pan-American infrastructure that can potentially involve it: in this figure, mass movements detected both through field surveys and with the application of KDE algorithm to SAR data are reported. In the bottom right corner, the types of movements of detected landslides are summarized.

Table 2. Methods of detection for the landslides in the buffer zone surrounding the Pan-American Highway.

	Rotational Slide	Planar Slide	Fall	Topple	Total
Field-surveyed landslides	6	3	20	1	30
Remote-sensed landslides	82	29	-	-	111

The mapped landslides cover a total area of about 6 km^2. Referring to the classification proposed by Cruden and Varnes [59] and Hungr et al. [60], recognized slope failures were grouped into the following principal landslide types and a percentage distribution analysis was then performed (Figure 7).

A high number of mass movements can be classified as rotational slides (88–62.4%), followed by falls (20–14.2%), planar slides (32–22.7%), and topples (1–0.7%), which are typical phenomena affecting mountainous and hilly areas, commonly related to the interaction between the geostructural features and rainfall events. The most common landslide types along the road axis are rotational slides and falls. In fact, the Pan-American, for long stretches, runs parallel to the Azogues Formation, composed mainly of conglomerates.

5.2. Identification of Potential Rockfall Sectors with QPROTO

The results implemented in QPROTO provide different output maps directly displayed in the QGIS interface and with a preset chromatic scale that facilitates the visualization. For this application, three classes were identified: blue color is associated with the lowest potential slope failure class, yellow color indicates the moderate class, and red color is used to highlight the higher one. For the stretch of the Pan-American Highway considered, about 7 km were found to be exposed to landslides (Figures 8–11).
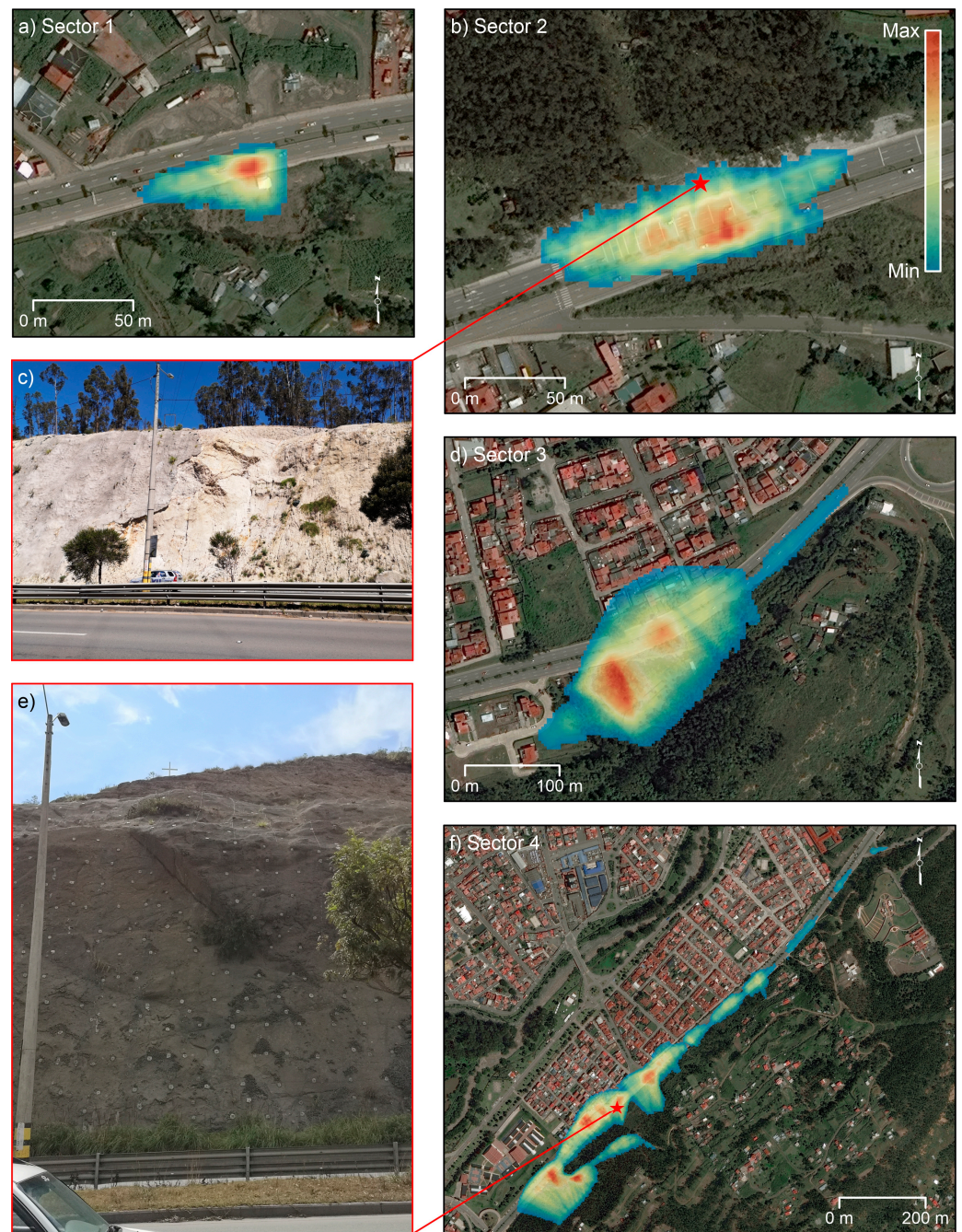
Figure 8. Outcomes of QPROTO algorithm for sector n° 1 (**a**), 2 (**b**), 3 (**d**), 4 (**f**) with different classes of potential rockfall runout occurrences; pictures (**c**,**e**) show the slopes prone to collapse for sector 2 and sector 4, respectively.
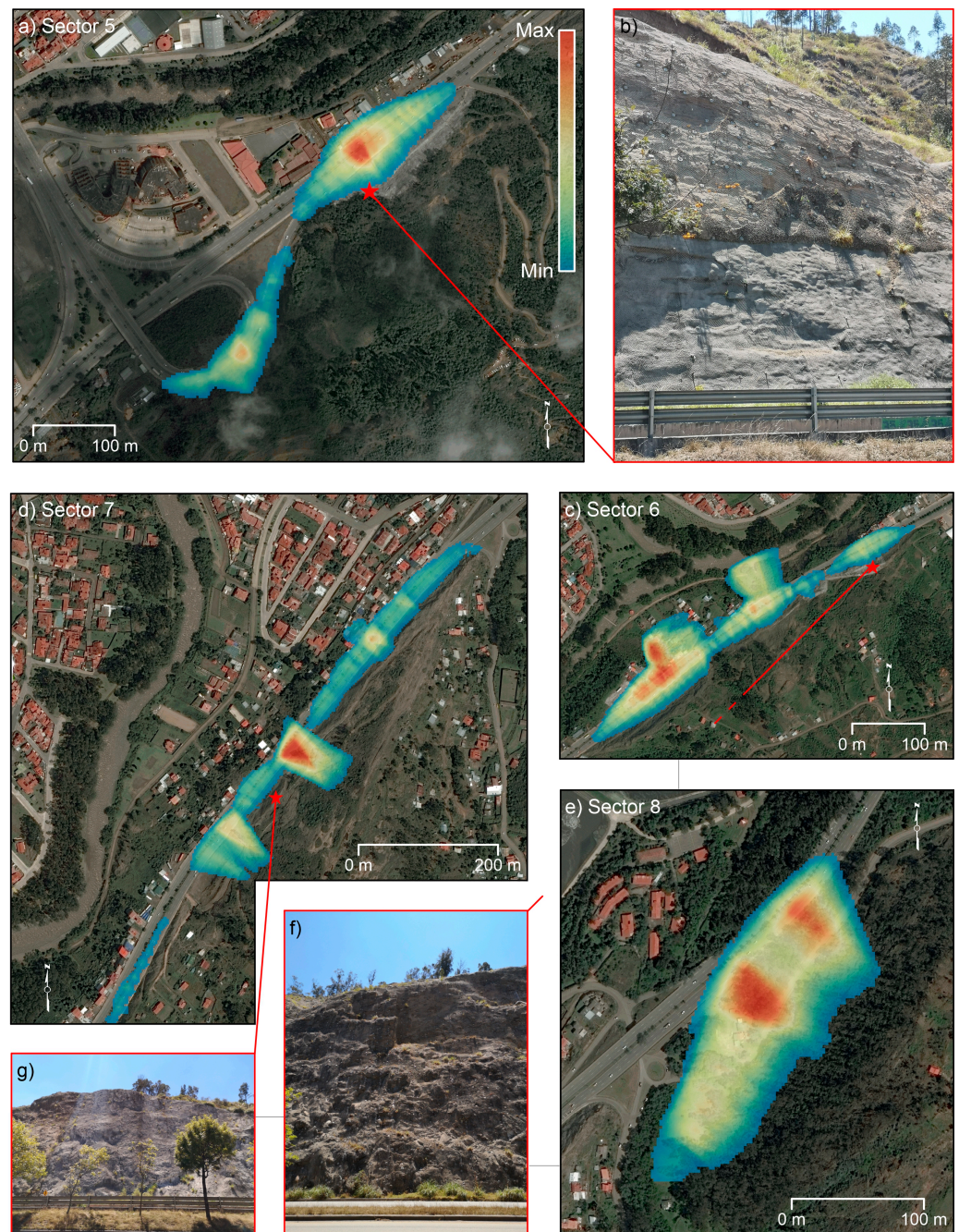
Figure 9. Outcomes of QPROTO algorithm for sector n° 5 (**a**), 6 (**c**), 7 (**d**), 8 (**e**) with different classes of potential rockfall runout occurrences; pictures (**b**,**f**,**g**) show the slopes prone to collapse for sectors 5, 6, and 7, respectively.
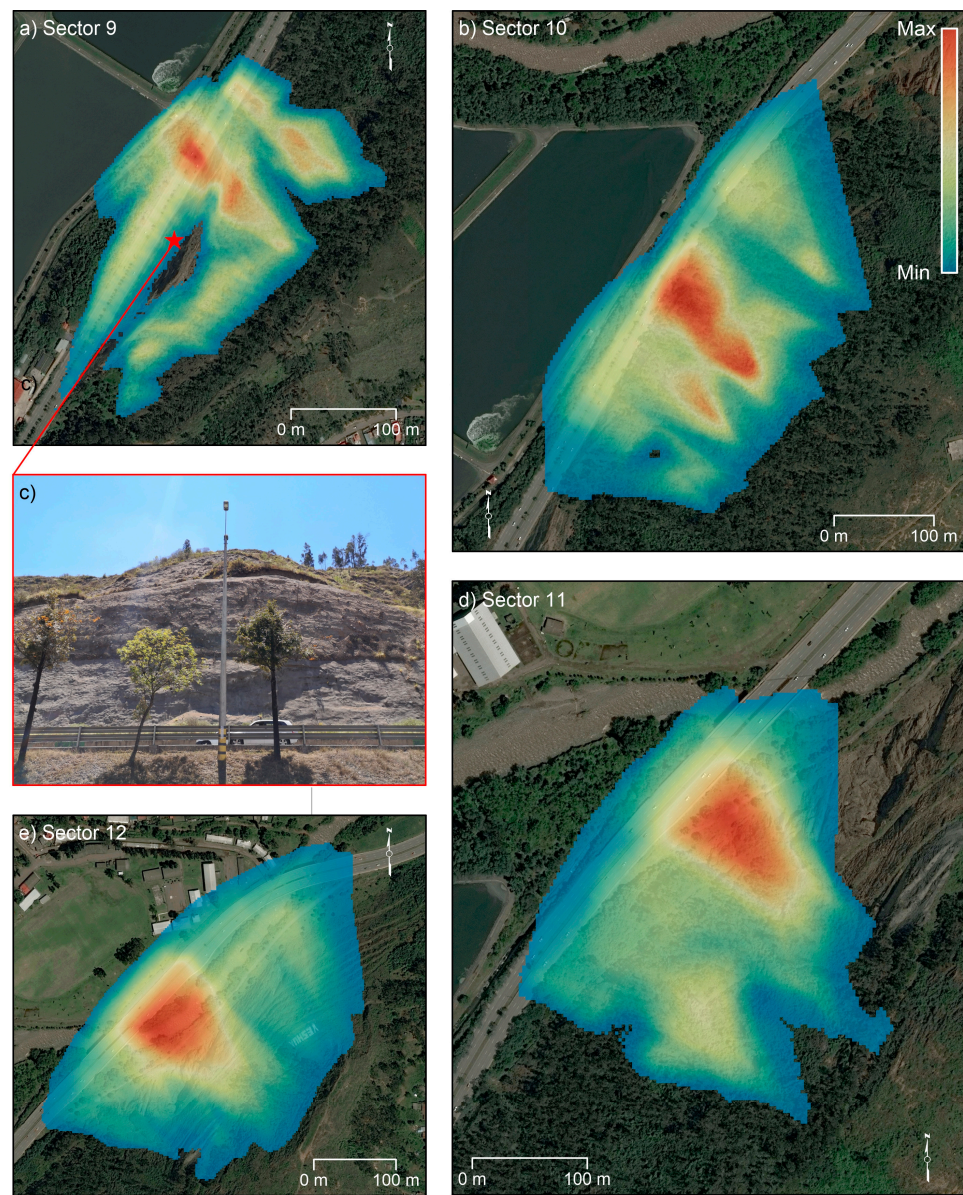
Figure 10. Outcomes of QPROTO algorithm for sector n° 9 (**a**), 10 (**b**), 11 (**d**), 12 (**e**) with different classes of potential rockfall runout occurrences; picture (**c**) shows the slopes prone to collapse for sector 9.
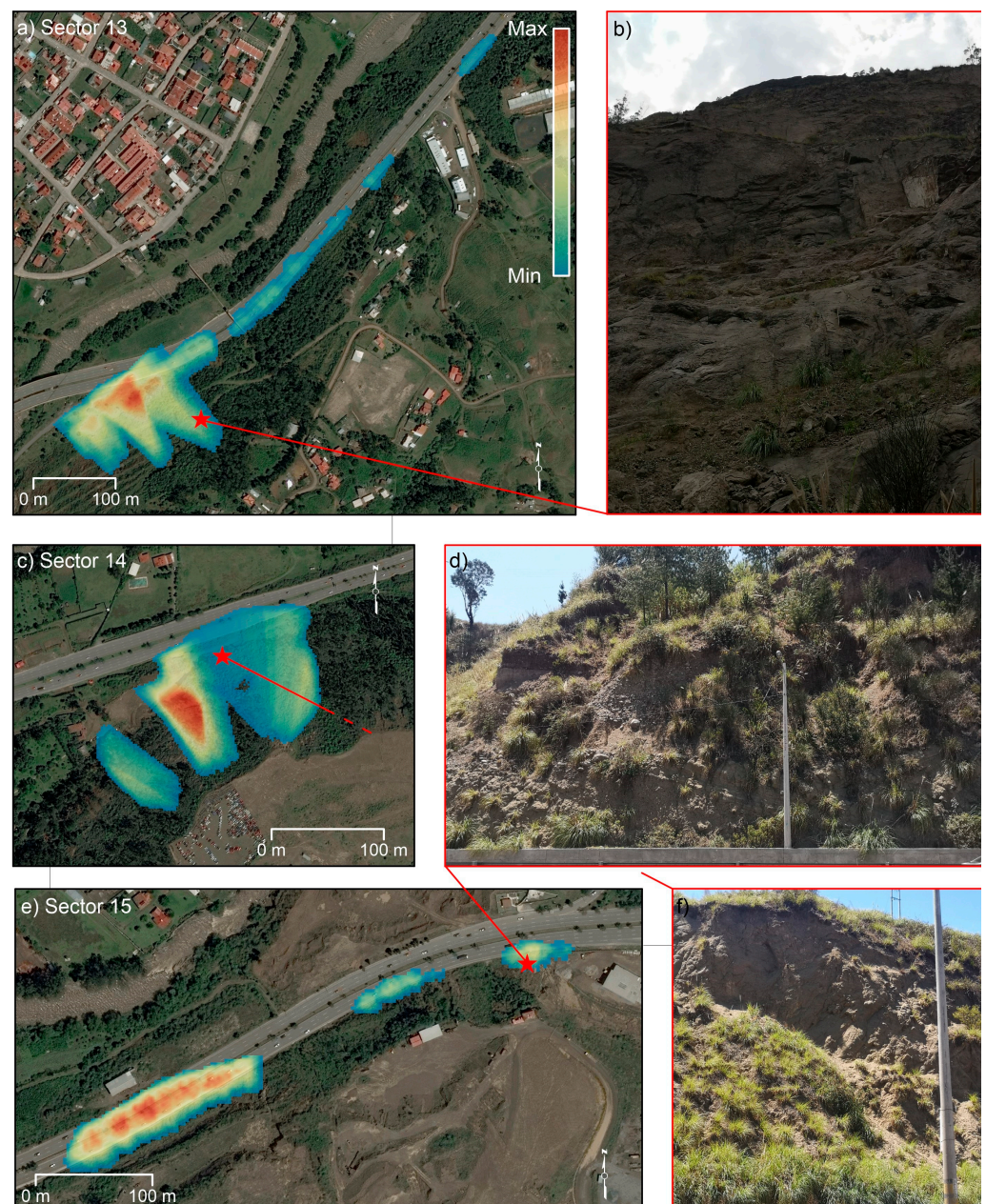
Figure 11. Outcomes of QPROTO algorithm for sector n° 13 (**a**), 14 (**c**), and 15 (**e**) with different classes of potential rockfall runout occurrences; the pictures (**b,d,f**) show the slopes prone to collapse for sector numbers 13, 14, and 15, respectively.

In detail, about 6 km of the highway is potentially intersected by low- to medium-intensity rockfall runout, with 1 km by high-intensity occurrence of boulder invasion. Among the different sectors identified, only one sector (i.e., 14) is not intersected by high-intensity rockfall runout (Figure 12). All the other sectors are prone to be intersected by low-, moderate-, and high-intensity mass movements.
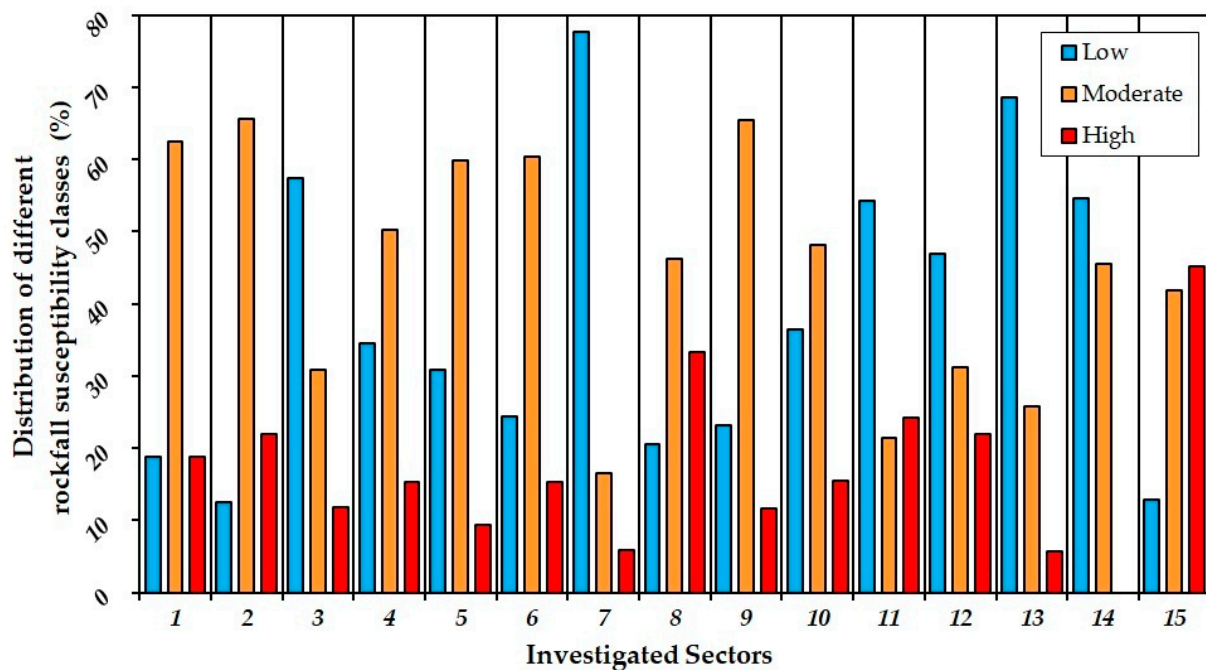
Figure 12. Summarized outcomes of QPROTO plugin. Blue, orange, and red colors indicate the "low", "moderate", and "high" degree of rockfall runout invasion for each sector analyzed, respectively.

Among the 15 sectors identified, eight are most affected by moderate intensity rockfalls and six are the most suitable to low intensity. Sector number 15, located in the northeastern part of the study area, shows the highest number of occurrences (Figure 12). The highest intensity class is present almost along the whole track studied, and only in three cases is it less than 10% of all the susceptible areas identified through QPROTO plugin (i.e., sectors 5, 7, 13, 14). Hence, this approach has made it possible to recognize that the propensity for rapid phenomena instability, such as rockfalls, is present along the entire Pan-American Highway.

6. Discussion

Natural and anthropogenic slope failures are frequent in the Andes of Ecuador, causing severe and constant issues [67]. Regrettably, only a few studies have been carried out about the relationship between the structures to be built, or already present, and the natural phenomena. As for this case study, the produced LIM emphasizes how landslides represent the principal hazard within the study area and how such phenomena interact with the Pan-American Highway. The proposed methodological approaches allowed the investigation of different types of mass movements that involve the infrastructure. The analyses benefited from the availability of medium-resolution DInSAR data (Sentinel-1), and information of QPROTO tool to identify detachment and runout areas. Both the results obtained with these two methods were used to validate and integrate the surveyed landslides.

Although the DInSAR technique is characterized by some limitations, such as the underestimation of the real vector of motion due to the acquisition mode, and the capability to detect only slow or extremely slow deformations, this study has confirmed its great value to monitor deformations in the study area in near real time and that it could be used for the monitoring of the whole infrastructure network thanks to high spatial and temporal resolution. Such a technique can help in the identification of stretches and sections along linear infrastructures affected by active deformations, providing information on spatial and temporal evolution. Therefore, DInSAR allows periodically to update boundary and state of activity of ground instability phenomena reported in the LIM. High spatial and temporal resolution of SAR images enables, nowadays, to investigate deformations and structural behavior both of large areas and single parts of infrastructure (with revisiting

time of 6 days). Furthermore, the DInSAR technique allowed to detect and monitor possible precursory phenomena highlighted by local accelerations in SCS time series. Rockfalls are usually characterized by fast velocities and affect high slope angles [68], reducing the suitability of spaceborne DInSAR methodologies.

Subsequently, to perform a quantitative analysis of the areas potentially affected by rockfalls, the QPROTO plugin was used. As input, slope analysis to identify areas with acclivity greater than 45 degrees was performed, allowing quick identification of the areas with greater rockfall properties. The subdivision of the various sectors also made it possible to choose in which areas to carry out priority stabilization interventions. Thanks to this application, it was possible to ascertain that of the total 22 km, about 7 km are affected by rockfall phenomena. The propensity of the lithologies to collapse is stressed by the poor cohesion which considerably increases the probability of detachment of conglomerates and blocks of rocks. These phenomena mainly manifest themselves where anthropic actions have occurred, such as cutting linked to the construction of infrastructures.

The combined use of DInSAR techniques and the QPROTO tool allowed the identification of both slow and rapid kinematic landslides. Thus, the Pan-American Highway can be divided according to different occurrence probability and to the various types of landslides that could occur. This sectorialization makes it possible to take action where the critical issues are greater without having to operate on the entire road track. The securing of instability phenomena which could affect the infrastructure, during their initial stage, allows to preserve the huge economic resources that were employed in the past to reroute the original road axis when no longer usable. In fact, in recent decades, the irreversible phenomena occurrence has caused road system interruption with consequent socioeconomic problems. Over the years, landslides have led to the closure of road sections and, in some cases, also involved motorists. Furthermore, it is not uncommon to notice substantial deviations of the road path due to these events, trying to circumvent phenomena of very high magnitudes.

For this purpose, given the widespread diffusion of new technologies, such as smartphones, an upgrade procedure can be implemented via app for the instability phenomena occurring along the Pan-American Highway. In this way, a first level of information on landslides' status and activity can be reported by the population. Subsequently, technicians should verify the received information, planning the most suitable interventions. This strategy would make it possible to promptly intervene where instability phenomena occur. The obtained outcomes will be used in future applications based on statistical modeling to achieve a susceptibility map of the whole region.

Therefore, the implementation of a monitoring system that allows to intervene in near real time, and at the same time provide quantitative information, is an instrument of fundamental importance.

Pursuing an optimization of economic and technical resources, it is important to underline that the proposed methodology does not require expensive costs. The use of DInSAR techniques could reduce the high costs for ordinary road maintenance, which are valued today between USD 200,000 and USD 300,000 per kilometer (https://ww2.elmercurio.com.ec/2020/08/07/el-nuevo-ingreso-sur-a-cuenca-tendra-peajes-y-sera-concesionado/; https://ww2.elmercurio.com.ec/2018/07/13/el-gobierno-nacional-entrego-la-reconstruccion-de-la-cuenca-azogues-biblian-se-intervinieron-42-km/; https://paisenvivo.com/se-inici-estudios-para-ampliacin-de-autopista-cuenca-azogues-biblin/, accessed on 15 March 2021). In fact, adding the costs of the methodologies used in this study, it is calculated that the monitoring and field survey activities for instability phenomena detection in the investigated sectors cost few tens of thousands of dollars. The costs are reduced because the SENTINEL-1 images are free of charge, and at the same time the DInSAR techniques and the QPROTO plugin are completely accessible through the use of free software. This would allow stakeholders to implement a near real-time monitoring system to identify the most prone road sections to landslides.

7. Conclusions

The paper presents a cognitive tool depicting slope dynamics in terms of actively moving and potential landslides affecting users' safety and the correct functionality of a segment of the Pan-American Highway which connects the cities of Cuenca and Azogues. The tool consists of a combination of a slow-moving landslide inventory and rockfall propagation analysis comprehensively depicting landslide potential over the analyzed highway segment. Such products were derived using specifically implemented procedure based on both field-based and PS-driven slow moving landslide inventory and reduced complexity rockfall propagation modeling. The obtained inventory indicated the presence of 141 landslides affecting or potentially influencing the highway segment. Rockfall analysis indicates the presence of a number of critical sectors of the highway for which a high propagation potential does exist. The implemented procedure, providing an overview of the landslide potential of the study area, can be considered as an operative landslide awareness system having the potential to increase safety of transport infrastructure and to support resilience development in the area. The Andean region of Ecuador, where the city of Cuenca is located, is prone to landslides due to its geological and geomorphological peculiarities. Such proneness, in combination with the fast development of the urban areas, has been causing increased physical damage and huge economic losses. In this context, the knowledge of landslide potential is of great importance, especially if supported by operational monitoring. The developed procedure, based on updatable PS data, is an easy upgrade to account for this aspect, also providing support to natural hazards management and cost-effective mitigation planning. In this perspective, the association of mapped landslide data with predicted rockfall propagation zones represents a major advance.

References

1. Fassin, D.; Vasquez, P. Humanitarian Exception as the Rule: The Political Theology of the 1999 Tragedia in Venezuela. *Am. Ethnol.* **2005**, *32*, 389–405. [CrossRef]
2. Vranken, L.; Van Turnhout, P.; Van Den Eeckhaut, M.; Vandekerckhove, L.; Poesen, J. Economic Valuation of Landslide Damage in Hilly Regions: A Case Study from Flanders, Belgium. *Sci. Total Environ.* **2013**, *447*, 323–336. [CrossRef]
3. Infante, D.; Di Martire, D.; Calcaterra, D.; Miele, P.; Scotto di Santolo, A.; Ramondini, M. Integrated Procedure for Monitoring and Assessment of Linear Infrastructures Safety (I-Pro MONALISA) Affected by Slope Instability. *Appl. Sci.* **2019**, *9*, 5535. [CrossRef]
4. Leroi, E. Science versus Economy and Sociology: Balanced Modeling for a Balanced Protection... How to Fit the Needs of the Society? *Ital. J. Geosci.* **2013**, *132*, 330–340. [CrossRef]
5. Anderson, M.G.; Holcombe, E. *Community-Based Landslide Risk Reduction: Managing Disasters in Small Steps*; World Bank Publications: Washington, DC, USA, 2013, ISBN 978-0-8213-9491-5.
6. Martino, S.; Bozzano, F.; Caporossi, P.; D'Angiò, D.; Della Seta, M.; Esposito, C.; Fantini, A.; Fiorucci, M.; Giannini, L.M.; Iannucci, R. Impact of Landslides on Transportation Routes during the 2016–2017 Central Italy Seismic Sequence. *Landslides* **2019**, *16*, 1221–1241. [CrossRef]
7. Dragos, K.; Smarsly, K. Decentralized infrastructure health monitoring using embedded computing in wireless sensor networks. In *Dynamic Response of Infrastructure to Environmentally Induced Loads*; Springer: Berlin, Germany, 2017; pp. 183–201.

8.   Fornaro, G.; Reale, D.; Verde, S. Potential of SAR for Monitoring Transportation Infrastructures: An Analysis with the Multi-Dimensional Imaging Technique. *J. Geophys. Eng.* **2012**, *9*, S1–S9. [CrossRef]

9.   Corominas, J.; van Westen, C.; Frattini, P.; Cascini, L.; Malet, J.-P.; Fotopoulou, S.; Catani, F.; Van Den Eeckhaut, M.; Mavrouli, O.; Agliardi, F.; et al. Recommendations for the Quantitative Analysis of Landslide Risk. *Bull. Eng. Geol. Env.* **2014**, *73*, 209–263. [CrossRef]

10.   Meyer, V.; Becker, N.; Markantonis, V.; Schwarze, R.; van den Bergh, J.C.J.M.; Bouwer, L.M.; Bubeck, P.; Ciavola, P.; Genovese, E.; Green, C.; et al. Review Article: Assessing the Costs of Natural Hazards—State of the Art and Knowledge Gaps. *Nat. Hazards Earth Syst. Sci.* **2013**, *13*, 1351–1373. [CrossRef]

11.   Alexander, D. Vulnerability to Landslides. In *Landslide Hazard Risk*; John Wiley & Sons, Inc.: Hoboken, NJ, USA, 2005; pp. 175–198.

12.   Papathoma-Köhle, M.; Kappes, M.; Keiler, M.; Glade, T. Physical Vulnerability Assessment for Alpine Hazards: State of the Art and Future Needs. *Nat. Hazards* **2011**, *58*, 645–680. [CrossRef]

13.   Franceschetti, G.; Migliaccio, M.; Riccio, D.; Schirinzi, G. SARAS: A Synthetic Aperture Radar(SAR) Raw Signal Simulator. *IEEE Trans. Geosci. Remote Sens.* **1992**, *30*, 110–123. [CrossRef]

14.   Bakon, M.; Perissin, D.; Lazecky, M.; Papco, J. Infrastructure Non-Linear Deformation Monitoring via Satellite Radar Interferometry. *Procedia Technol.* **2014**, *16*, 294–300. [CrossRef]

15.   Poreh, D.; Iodice, A.; Riccio, D.; Ruello, G. Railways' Stability Observed in Campania (Italy) by InSAR Data. *Eur. J. Remote Sens.* **2016**, *49*, 417–431. [CrossRef]

16.   Orellana, F.; Delgado Blasco, J.M.; Foumelis, M.; D'Aranno, P.J.V.; Marsella, M.A.; Di Mascio, P. DInSAR for Road Infrastructure Monitoring: Case Study Highway Network of Rome Metropolitan (Italy). *Remote Sens.* **2020**, *12*, 3697. [CrossRef]

17.   North, M.; Farewell, T.; Hallett, S.; Bertelle, A. Monitoring the Response of Roads and Railways to Seasonal Soil Movement with Persistent Scatterers Interferometry over Six UK Sites. *Remote Sens.* **2017**, *9*, 922. [CrossRef]

18.   Zhu, M.; Wan, X.; Fei, B.; Qiao, Z.; Ge, C.; Minati, F.; Vecchioli, F.; Li, J.; Costantini, M. Detection of Building and Infrastructure Instabilities by Automatic Spatiotemporal Analysis of Satellite SAR Interferometry Measurements. *Remote Sens.* **2018**, *10*, 1816. [CrossRef]

19.   Peduto, D.; Giangreco, C.; Venmans, A.A. Differential Settlements Affecting Transition Zones between Bridges and Road Embankments on Soft Soils: Numerical Analysis of Maintenance Scenarios by Multi-Source Monitoring Data Assimilation. *Transp. Geotech.* **2020**, *24*, 100369. [CrossRef]

20.   Bekaert, D.P.S.; Handwerger, A.L.; Agram, P.; Kirschbaum, D.B. InSAR-Based Detection Method for Mapping and Monitoring Slow-Moving Landslides in Remote Regions with Steep and Mountainous Terrain: An Application to Nepal. *Remote Sens. Environ.* **2020**, *249*, 111983. [CrossRef]

21.   Montalti, R.; Solari, L.; Bianchini, S.; Soldato, M.D.; Raspini, F.; Casagli, N. A Sentinel-1-Based Clustering Analysis for Geo-Hazards Mitigation at Regional Scale: A Case Study in Central Italy. *Geomat. Nat. Hazards Risk* **2019**, *10*, 2257–2275. [CrossRef]

22.   Zhao, C.; Kang, Y.; Zhang, Q.; Lu, Z.; Li, B. Landslide Identification and Monitoring along the Jinsha River Catchment (Wudongde Reservoir Area), China, Using the InSAR Method. *Remote Sens.* **2018**, *10*, 993. [CrossRef]

23.   Mignelli, C.; Peila, D.; Russo, S.L.; Ratto, S.M.; Broccolato, M. Analysis of Rockfall Risk on Mountainside Roads: Evaluation of the Effect of Protection Devices. *Nat. Hazards* **2014**, *73*, 23–35. [CrossRef]

24.   Cloutier, C.; Locat, J.; Mayers, M.; Noël, F.; Turmel, D.; Jacob, C.; Dorval, P.; Bossé, F.; Gionet, P.; Jaboyedoff, M. An Integrated Management Tool for Rockfall Evaluation along Transportation Corridors: Description and Objectives of the ParaChute Research Project. In Proceedings of the GEOQuébec 2015, Québec City, QC, Canada, 21–23 September 2015.

25.   Donnini, M.; Napolitano, E.; Salvati, P.; Ardizzone, F.; Bucci, F.; Fiorucci, F.; Santangelo, M.; Cardinali, M.; Guzzetti, F. Impact of Event Landslides on Road Networks: A Statistical Analysis of Two Italian Case Studies. *Landslides* **2017**, *14*, 1521–1535. [CrossRef]

26.   Confuorto, P.; Di Martire, D.; Centolanza, G.; Iglesias, R.; Mallorqui, J.J.; Novellino, A.; Plank, S.; Ramondini, M.; Thuro, K.; Calcaterra, D. Post-Failure Evolution Analysis of a Rainfall-Triggered Landslide by Multi-Temporal Interferometry SAR Approaches Integrated with Geotechnical Analysis. *Remote Sens. Environ.* **2017**, *188*, 51–72. [CrossRef]

27.   Frodella, W.; Ciampalini, A.; Gigli, G.; Lombardi, L.; Raspini, F.; Nocentini, M.; Scardigli, C.; Casagli, N. Synergic Use of Satellite and Ground Based Remote Sensing Methods for Monitoring the San Leo Rock Cliff (Northern Italy). *Geomorphology* **2016**, *264*, 80–94. [CrossRef]

28.   Carlà, T.; Intrieri, E.; Raspini, F.; Bardi, F.; Farina, P.; Ferretti, A.; Colombo, D.; Novali, F.; Casagli, N. Perspectives on the Prediction of Catastrophic Slope Failures from Satellite InSAR. *Sci. Rep.* **2019**, *9*, 14137. [CrossRef] [PubMed]

29.   Di Napoli, M.; Di Martire, D.; Bausilio, G.; Calcaterra, D.; Confuorto, P.; Firpo, M.; Pepe, G.; Cevasco, A. Rainfall-Induced Shallow Landslide Detachment, Transit and Runout Susceptibility Mapping by Integrating Machine Learning Techniques and GIS-Based Approaches. *Water* **2021**, *13*, 488. [CrossRef]

30.   Volkwein, A.; Schellenberg, K.; Labiouse, V.; Agliardi, F.; Berger, F.; Bourrier, F.; Dorren, L.K.A.; Gerber, W.; Jaboyedoff, M. Rockfall Characterisation and Structural Protection—A Review. *Nat. Hazards Earth Syst. Sci.* **2011**, *11*, 2617–2651. [CrossRef]

31.   Chen, G.; Zheng, L.; Zhang, Y.; Wu, J. Numerical Simulation in Rockfall Analysis: A Close Comparison of 2-D and 3-D DDA. *Rock Mech. Rock Eng.* **2013**, *46*, 527–541. [CrossRef]

32.   Jaboyedoff, M.; Labiouse, V. Preliminary Estimation of Rockfall Runout Zones. *Nat. Hazards Earth Syst. Sci.* **2011**, *11*, 819–828. [CrossRef]

33. Castelli, M.; Torsello, G.; Vallero, G. Preliminary Modeling of Rockfall Runout: Definition of the Input Parameters for the QGIS Plugin QPROTO. *Geosciences* **2021**, *11*, 88. [CrossRef]

34. Scavia, C.; Barbero, M.; Castelli, M.; Marchelli, M.; Peila, D.; Torsello, G.; Vallero, G. Evaluating Rockfall Risk: Some Critical Aspects. *Geosciences* **2020**, *10*, 98. [CrossRef]

35. Plaza, G.; Zevallos, O.; Cadier, É. La Josefina Landslide Dam and Its Catastrophic Breaching in the Andean Region of Ecuador. In *Natural and artificial rockslide dams*; Springer: Berlin, Germany, 2011; pp. 389–406.

36. Di Martire, D.; Confuorto, P.; Frezza, A.; Ramondini, M.; Lòpez, A.V.; Del Rosso, M.P.; Sebastianelli, A.; Ullo, S.L. X-and C-Band SAR Data to Monitoring Ground Deformations and Slow-Moving Landslides for the 2016 Manta and Portoviejo Earthquake (Manabi, Ecuador). In Proceedings of the 2018 IEEE International Conference on Environmental Engineering (EE), Milan, Italy, 12–14 March 2018; pp. 1–6.

37. Sellers, C.; Rodas, R.; Carrasco, N.P.; De Stefano, R.; Di Martire, D.; Ramondini, M. Ground Deformation Monitoring of a Strategic Building Affected by Slow-Moving Landslide in Cuenca (Ecuador). In *European Workshop on Structural Health Monitoring*; Rizzo, P., Milazzo, A., Eds.; Springer International Publishing: Cham, Switzerland, 2021; pp. 149–158.

38. Muenchow, J.; Brenning, A.; Richter, M. Geomorphic Process Rates of Landslides along a Humidity Gradient in the Tropical Andes. *Geomorphology* **2012**, *139–140*, 271–284. [CrossRef]

39. Schuster, R.L.; Highl, L.M. *Socioeconomic and Environmental Impacts of Landslides in the Western Hemisphere*; USGS Open-File Report, 01–276; U.S. Geological Survey: Denver, CO, USA, 2001.

40. Basabe, P.; Almeida, E.; Ramon, P.; Zeas, R.; Alvarez, L. Avance En La Prevención de Desastres Naturales En La Cuenca Del Río Paute, Ecuador. *Bull. De L'institut Fr. D'études Andin.* **1996**, *25*, 443–458.

41. Bignami, D.F.; Dragoni, A.; Menduni, G. Assessing and Improving Flood and Landslide Community Social Awareness and Engagement via a Web Platform: The Case of Italy. *Int. J. Disaster Risk Sci.* **2018**, *9*, 530–540. [CrossRef]

42. *Estudios de Ingeniería Definitivos de la Carretera Cuenca-Azogues-Biblián*; Ministerio de Transportes y Obras Públicas: Quito, Ecuador, 2019; p. 71.

43. LITHERLAND, M. The Metamorphic Belts of Ecuador. *Br. Geol. Surv. Overseas Mem.* **1994**, *11*, 1–147.

44. Dunkley, P.N.; Gaibor, A. Mapa Geológico de La Cordillera Occidental Del Ecuador Entre 2-3 S., Escala 1/200.000. *Codigem-Minist. De Energía Y Minas-Br. Geol. Surv. Publs. Quito* **1998**.

45. Pratt, W.; Figueroa, J.; Flores, B. *Geology of the Cordillera Occidental of Ecuador between 3°00′ and 4°00′S*; World Bank Mining Development and Environmental Control Project: Quito, Ecuador, 1997; p. 58.

46. Feininger, T.; Bristow, C.R. Cretaceous and Paleogene Geologic History of Coastal Ecuador. *Geol. Rundsch.* **1980**, *69*, 849–874. [CrossRef]

47. Noblet, C.; Lavenu, A.; Marocco, R. Concept of Continuum as Opposed to Periodic Tectonism in the Andes. *Tectonophysics* **1996**, *255*, 65–78. [CrossRef]

48. Hungerbühler, D.; Steinmann, M.; Winkler, W.; Seward, D.; Egüez, A.; Peterson, D.E.; Helg, U.; Hammer, C. Neogene Stratigraphy and Andean Geodynamics of Southern Ecuador. *Earth-Sci. Rev.* **2002**, *57*, 75–124. [CrossRef]

49. Faucher, B.; Vernet, R.; Bizon, G.; Bizon, J.; Grekoff, N.; Lys, M.; Sigal, J. Sedimentary Formations in Ecuador. A Stratigraphic and Micropaleontological Survey. Bureau d'Études Industrielles et Coopération de l'Institut Français du Pétrole (BEICIP). 1971.

50. Bristow, C.R. *Sociedad Ecuatoriana de Geología y Geofísica. Guide to the Geology of the Cuenca Basin, Southern Ecuador*; Ecuadorian Geological and Geophysical Society: Quito, Ecuador, 1973.

51. Fiorillo, F.; Guerriero, L.; Capobianco, L.; Pagnozzi, M.; Revellino, P.; Russo, F.; Guadagno, F.M. Inventory of Vietri-Maiori Landslides Induced by the Storm of October 1954 (Southern Italy). *J. Maps* **2019**, *15*, 530–537. [CrossRef]

52. Galli, M.; Ardizzone, F.; Cardinali, M.; Guzzetti, F.; Reichenbach, P. Comparing Landslide Inventory Maps. *Geomorphology* **2008**, *94*, 268–289. [CrossRef]

53. Guerriero, L.; Confuorto, P.; Calcaterra, D.; Guadagno, F.M.; Revellino, P.; Di Martire, D. PS-Driven Inventory of Town-Damaging Landslides in the Benevento, Avellino and Salerno Provinces, Southern Italy. *J. Maps* **2019**, *15*, 619–625. [CrossRef]

54. Scaioni, M.; Longoni, L.; Melillo, V.; Papini, M. Remote Sensing for Landslide Investigations: An Overview of Recent Achievements and Perspectives. *Remote Sens.* **2014**, *6*, 9600–9652. [CrossRef]

55. Santangelo, M.; Marchesini, I.; Bucci, F.; Cardinali, M.; Fiorucci, F.; Guzzetti, F. An Approach to Reduce Mapping Errors in the Production of Landslide Inventory Maps. *Nat. Hazards Earth Syst. Sci.* **2015**, *15*, 2111–2126. [CrossRef]

56. Ferretti, A.; Prati, C.; Rocca, F. Permanent Scatterers in SAR Interferometry. *IEEE Trans. Geosci. Remote Sens.* **2001**, *39*, 8–20. [CrossRef]

57. Mora, O.; Mallorqui, J.J.; Broquetas, A. Linear and Nonlinear Terrain Deformation Maps from a Reduced Set of Interferometric SAR Images. *IEEE Trans. Geosci. Remote Sens.* **2003**, *41*, 2243–2253. [CrossRef]

58. Iglesias, R.; Mallorqui, J.J.; Monells, D.; López-Martínez, C.; Fabregas, X.; Aguasca, A.; Gili, J.A.; Corominas, J. PSI Deformation Map Retrieval by Means of Temporal Sublook Coherence on Reduced Sets of SAR Images. *Remote Sens.* **2015**, *7*, 530–563. [CrossRef]

59. Lu, P.; Casagli, N.; Catani, F.; Tofani, V. Persistent Scatterers Interferometry Hotspot and Cluster Analysis (PSI-HCA) for Detection of Extremely Slow-Moving Landslides. *Int. J. Remote Sens.* **2012**, *33*, 466–489. [CrossRef]

60. Di Martire, D.; Tessitore, S.; Brancato, D.; Ciminelli, M.G.; Costabile, S.; Costantini, M.; Graziano, G.V.; Minati, F.; Ramondini, M.; Calcaterra, D. Landslide Detection Integrated System (LaDIS) Based on in-Situ and Satellite SAR Interferometry Measurements. *Catena* **2016**, *137*, 406–421. [CrossRef]

61. Ammirati, L.; Mondillo, N.; Rodas, R.A.; Sellers, C.; Di Martire, D. Monitoring Land Surface Deformation Associated with Gold Artisanal Mining in the Zaruma City (Ecuador). *Remote Sens.* **2020**, *12*, 2135. [CrossRef]

62. Cruden, D.M.; Varnes, D.J. *Landslides: Investigation and Mitigation. Chapter 3—Landslide Types and Processes*; Transportation Research Board Special Report 247; Transportation Research Board: Washington, DC, USA, 1996; pp. 36–75.

63. Hungr, O.; Leroueil, S.; Picarelli, L. The Varnes Classification of Landslide Types, an Update. *Landslides* **2014**, *11*, 167–194. [CrossRef]

64. Colesanti, C.; Ferretti, A.; Novali, F.; Prati, C.; Rocca, F. SAR Monitoring of Progressive and Seasonal Ground Deformation Using the Permanent Scatterers Technique. *IEEE Trans. Geosci. Remote Sens.* **2003**, *41*, 1685–1701. [CrossRef]

65. Onofri, R.; Candian, C. *Indagini Sui Limiti Di Massima Invasione Dei Blocchi Rocciosi Franati Durante Il Sisma Del Friuli Del 1976: Considerazioni Sulle Opere Di Difesa*; Università Degli Studi Trieste: Milan, Italy, 1979.

66. Saroglou, C. GIS-Based Rockfall Susceptibility Zoning in Greece. *Geosciences* **2019**, *9*, 163. [CrossRef]

67. Blodgett, T.A.; Blizard, C.; Isacks, B.L. Andean landslide hazards. In *Geomorphological Hazards in High Mountain Areas*; Springer: Berlin, Germany, 1998; pp. 211–227.

68. Notti, D.; Herrera, G.; Bianchini, S.; Meisina, C.; García-Davalillo, J.C.; Zucca, F. A Methodology for Improving Landslide PSI Data Analysis. *Int. J. Remote Sens.* **2014**, *35*, 2186–2214. [CrossRef]